at high surface temperatures. In contrast, a mechanism based on desorption via the interdimer pathway matches the experimental data nicely (Fig. 4, middle panel). The increased population of the intradimer configuration (separation = 0) relative to that for a configuration with a separation of two dimers is attributed to stabilization of the intradimer configuration by the pairing energy described above. We have also analyzed the configurations found in regions of the surface where a greater amount of hydrogen has been desorbed (nearer the center of the laser beam). The results are similar, but experimental observation and model prediction both show a somewhat increased population of the intradimer configuration. This shift arises from the enhanced thermal diffusivity of the adsorbed hydrogen associated with the increased surface temperature.

From the direct imaging of the sites left empty by the laser-induced recombinative desorption of H_2 from the Si(001) surface, we conclude that an interdimer pathway is operative. This finding appears to contradict the observed distribution of hydrogen adatoms after a conventional thermal desorption process (*17*). As discussed above, we understand the discrepancy simply in terms of the rearrangement of the hydrogen atoms by thermal diffusion during the course of the conventional heating cycle. More informative is a comparison of our result for the microscopic pathway for recombinative desorption with the behavior of the time-reversed process of dissociative adsorption of hydrogen. This latter process has been investigated extensively, and recent experiments indicate the existence of an interdimer pathway (*19, 23–26*). Indeed, direct evidence for the interdimer adsorption pathway has been obtained in our laboratory in a real-space STM study (*16*). These experimental results are also consistent with the latest theoretical investigations of the system (*25, 27*).

One might thus be tempted to view the result of the current experiment as an unavoidable consequence of the principle of detailed balance between the reverse processes of adsorption and desorption. This, however, would not be a valid inference. As is generally the case in surface science investigations, the adsorption and desorption measurements were performed under very different conditions. In addition to the fact that neither the adsorption nor the desorption experiments were actually conducted at equilibrium, the experiments probed distinct regimes of hydrogen surface coverage, surface temperature, and kinetic energy of the gas-phase H_2 molecules. Indeed, for this system, a comparison of the kinetic energy dependence of adsorption data taken at low coverage and temperature (*28*) with prior desorption measurements conducted in the high coverage and temperature regime (*29*) yielded certain departures from the predictions of detailed balance. One might then ask—given the complexity of the adsorption-desorption processes and, particularly, the role of displacements of the surface Si atoms—whether the same reaction pathway is followed in these very different regimes. Our experimental results answer this question in the affirmative and demonstrate the robustness of the interdimer adsorption-desorption pathway.

The STM technique illustrated here for the H/Si(001) system permits one to examine elementary reaction steps with substantial barriers that would otherwise be lost for STM analysis because of the presence of diffusion or other low-barrier processes. Potential applications of the method range from probing highly activated diffusion processes (such as ones occurring at steps and affecting crystal growth) to the atomically resolved analysis of product formation in heterogeneous catalysis.

References and Notes

1. J. Wintterlin, S. Völkening, T. V. W. Janssens, T. Zambelli, G. Ertl, *Science* **278**, 1931 (1997).
2. M. McEllistrem, M. Allgeier, J. J. Boland, *Science* **279**, 545 (1998).
3. S. Horch *et al.*, *Nature* **398**, 134 (1999).
4. C. Sachs, M. Hildebrand, S. Völkening, J. Wintterlin, G. Ertl, *Science* **293**, 1635 (2001).
5. R. A. van Santen, J. W. Niemantsverdriet, *Chemical Kinetics and Catalysis* (Plenum, New York, 1995).
6. G. Ertl, M. Neumann, *Z. Naturforsch.* **27A**, 1607 (1972).
7. J. P. Cowin, D. J. Auerbach, C. Becker, L. Wharton, *Surf. Sci.* **78**, 545 (1978).
8. R. B. Hall, A. M. DeSantolo, *Surf. Sci.* **137**, 421 (1984).
9. S. M. George, R. B. Hall, A. M. DeSantolo, *Surf. Sci.* **159**, L425 (1985).
10. M. Bonn *et al.*, *Science* **285**, 1042 (1999).
11. The earlier investigations have been discussed in several review articles (*12–14*); more recent studies are summarized in (*15, 16*).
12. K. W. Kolasinski, *Int. J. Mod. Phys. B* **21**, 2753 (1995).
13. D. J. Doren, *Adv. Chem. Phys.* **95**, 1 (1996).
14. U. Höfer, *Appl. Phys. A* **63**, 533 (1996).
15. W. Brenig, M. Hilf, *J. Phys. Condens. Matter* **13**, R61 (2001).
16. M. Dürr, Z. Hu, A. Biedermann, U. Höfer, T. F. Heinz, *Phys. Rev. Lett.* **88**, 046104 (2002).
17. J. J. Boland, *Phys. Rev. Lett.* **67**, 1539 (1991).
18. More quantitative analysis yields a peak surface temperature between 1300 and 1500 K, for which the initial desorption sites should be observable by STM for desorption times below 10 ns.
19. A. Biedermann, E. Knoesel, Z. Hu, T. F. Heinz, *Phys. Rev. Lett.* **83**, 1810 (1999).
20. In addition to pairs of unsaturated dangling bonds, some single dangling bonds are seen on the Si(001) surface after laser-induced thermal desorption. We are unable to explain these features by any form of hydrogen adatom diffusion after recombinative desorption, and we attribute these features to a slight uptake of hydrogen atoms into the bulk Si lattice (*30*). This weak process is not expected to influence the recombinative desorption of hydrogen investigated in this study.
21. J. H. G. Owen, D. R. Bowler, C. M. Goringe, K. Miki, G. A. D. Briggs, *Phys. Rev. B* **54**, 14153 (1996).
22. U. Höfer, Leping Li, T. F. Heinz, *Phys. Rev. B* **45**, 9485 (1992).
23. P. Kratzer, E. Pehlke, M. Scheffler, M. B. Raschke, U. Höfer, *Phys. Rev. Lett.* **81**, 5596 (1998).
24. F. M. Zimmermann, X. Pan, *Phys. Rev. Lett.* **85**, 618 (2000).
25. M. Dürr, M. B. Raschke, E. Pehlke, U. Höfer, *Phys. Rev. Lett.* **86**, 123 (2001).
26. M. Dürr, U. Höfer, *Phys. Rev. Lett.* **88**, 076107 (2002).
27. E. Pehlke, *Phys. Rev. B* **62**, 12932 (2000).
28. M. Dürr, M. B. Raschke, U. Höfer, *J. Chem. Phys.* **111**, 10411 (1999).
29. K. W. Kolasinski, W. Nessler, A. D. Meijere, E. Hasselbrink, *Phys. Rev. Lett.* **72**, 1356 (1994).
30. N. M. Johnson, C. Doland, F. Ponce, J. Walker, G. Anderson, *Physica B* **170**, 3 (1991).
31. Supported by the NSF, the Deutsche Forschungsgemeinschaft, the Deutscher Akademischer Austauschdienst (M.D.), and the Alexander von Humboldt Foundation (T.F.H.).

13 February 2002; accepted 29 April 2002

Microfluidic Control Using Colloidal Devices

Alex Terray, John Oakey,* David W. M. Marr*

By manipulating colloidal microspheres within customized channels, we have created micrometer-scale fluid pumps and particulate valves. We describe two positive-displacement designs, a gear and a peristaltic pump, both of which are about the size of a human red blood cell. Two colloidal valve designs are also demonstrated, one actuated and one passive, for the direction of cells or small particles. The use of colloids as both valves and pumps will allow device integration at a density far beyond what is currently achievable by other approaches and may provide a link between fluid manipulation at the macro- and nanoscale.

Microscale devices designed to accomplish specific tasks have repeatedly demonstrated superiority over their macroscale analogs (*1*, *2*). The advantages of such devices are due largely to unique transport properties resulting from laminar flows and vastly increased surface-to-volume ratios (*3*) and have enabled microscale sensors (*4*) and fabrication schemes (*5*) not possible on the macroscale. Additionally, microfluidic processes may be easily parallelized for high throughput (*6*) and require vastly smaller sample volumes, a major benefit for applications in which reagents or analytes are either hazardous or expensive (*7*). The utility, speed,

---

Chemical Engineering Department, Colorado School of Mines, Golden, CO 80401, USA.

*To whom correspondence should be addressed. E-mail: joakey@mines.edu (J.O.); dmarr@mines.edu (D.W.M.M.)

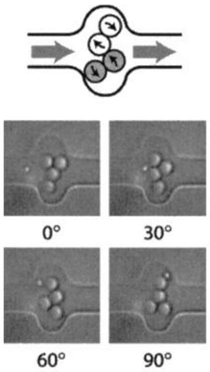

Fig. 1. Pump design illustrating lobe movement (the top pair rotate clockwise, the bottom counterclockwise). Also shown is 3-μm colloidal silica undergoing rotation at 2 Hz within a 6-μm channel. Frames are separated by two cycles to show movement of the 1.5-μm colloidal silica tracer particles. To create the pump, we first cured PDMS over a negative photoresist pattern created with conventional photolithography. The resulting elastomeric layer (~1 mm thick) was then placed upon a base fabricated from a block of Plexiglas designed to allow easy colloidal fluid introduction to the channel network through a syringe pump (Kd Scientific, KDS200, New Hope, PA). Holes through the PDMS membrane were then aligned with the fluid ports in the base with which the PDMS layer seals tightly and reversibly. A cover slip placed on top of the channel network created a tight, reversible seal and a closed microfluidic system. The optical trap consisted of a laser (Spectra Physics Millennia V, Mountain View, CA; 532-nm wavelength, typically operated at 0.8 W for actuation) and a microscope (Optiphot 150, Nikon) with an oil immersion 100× objective, numerical aperture = 1.3 (CFN plan fluor, Nikon) used to create a tight laser focus of ~1 μm and to observe the experiments. The piezoelectric mirror (Physik Instrumente, Karlsruhe, Germany) used to create the scanning trap was controlled by computer (Macintosh G3, Apple) with routines written in LabView (National Instruments, Austin, TX) and scanned at a rate of 50 to 100 Hz.

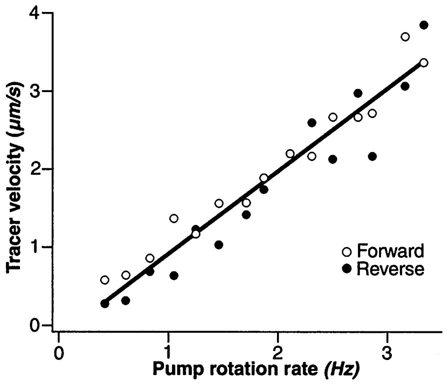

Fig. 2. Tracer particle velocity as a function of gear rotation rate for both forward and reverse directions. The line is a fit to guide the eye.

and performance of microsystems typically increase as the overall device size decreases. The need to pump and direct fluids at very small length scales, however, has long been the limiting factor in the development of microscale systems, thus generating a tremendous amount of interest in microfluidics development (*8*). As improved actuation techniques have become available, conventional valving and pumping schemes have been miniaturized, yet continue to dwarf microchannels and other chip-top features (*9*).

Recently, several approaches conceived explicitly for the microscale have been developed, including platforms based upon electrohydrodynamics (*10*), electroosmosis (*11*), interfacial phenomena (*12*, *13*), conjugated materials (*14*), magnetic materials (*15*), and multilayer soft lithography (*16*). Although these microfluid handling techniques enable functional devices on microscopic length scales, they also impose unique constraints upon potential device capability, flexibility, and performance. To fully integrate multiple fluidic processes within a single microsystem, methods for microfluid handling must be developed that can accommodate fluids of complex and dynamic composition and are of comparable size to that of the processes into which they are embedded.

Development of devices that can function at these length scales has focused on complex fabrication schemes for intricate components such as gears (*17*, *18*), cantilevers (*19*), and other microscale objects (*20*, *21*). The fabrication and actuation of these devices, however, has been limited to bulk environments external to the microfluidic geometries. Because no practical implementation scheme has been developed for their incorporation into functioning microfluidic systems, they have not realized their suggested potential as microfluidic pumps and valves. We avoid the complexities inherent in other approaches by using colloidal microspheres as the active flow-control element. These materials are an excellent choice because they can be synthesized at length scales easily transported through microfluidic networks and their surface chemistry may be readily altered. Colloidal silica, for example, is easily modified for dispersion in both aqueous and nonaqueous solvents and is well known for its biocompatibility, allowing its use in a host of microfluidic applications.

It has also been shown that colloids can be directly manipulated through the application of external fields. The processes of electrophoresis, dielectrophoresis, and magnetophoresis have all been used to control and influence the motion of small particles in solution. Particularly useful for our preliminary studies, however, is the technique of optical trapping, which has become popular because it allows the direct manipulation of individual colloids. This noncontact, noninvasive technique eliminates the need to physically interface to the macroscopic world and allows for the manipulation of complex asymmetric objects or multiple objects at once, as would be required for the actuation of a microfluidic valve or pump.

For multiple trap generation, we used a scanning approach in which a piezoelectric mirror is translated to rapidly reflect a laser beam in a desired pattern. If the piezoelectric mirror is scanned over the desired pattern at a frequency greater than that associated with Brownian time scales, a time-averaged trapping pattern is created. Through the application of this technique, known as scanning laser optical trapping (SLOT) (*22*, *23*), we are able to rearrange microspheres into functional structures and subsequently actuate these structures to generate microfluidic pumping and valving. However, using an optical actuation scheme and transmission microscopy to monitor device performance requires a method for the creation of channels at single-micrometer length scales in a transparent housing. Because of this requirement, we applied soft lithography techniques, pioneered by the Whitesides group, which allow for the inexpensive fabrication of microfluidic networks in poly(dimethylsiloxane) (PDMS), an optically transparent elastomer (*3*, *24*–*26*).

Working at microscopic length scales offers unique challenges for colloidal pump design. This is illustrated through calculation of the Reynolds number, $Re = \rho v D/\eta$, where for colloidal length scales in aqueous solutions, $\rho = 1$ g/cm^3, $\eta = 0.01$ g/cm·s, $D \approx 5$ μm, and $v \approx 5$ μm/s, giving $Re \approx 10^{-5} \ll 1$ and corresponding to laminar flow. Under these circumstances, fluid flow is fully reversible, and pump designs that rely on centrifugal action, such as impeller-type approaches, are inappropriate. For this reason, our designs are based on positive-displacement pumping techniques that operate by imparting forward motion to individual plugs of fluid.

Our first design is a two-lobe gear pump in which small, trapped pockets of fluid are directed through a specially designed cavity fabricated in a microchannel by rotating two colloidal dumbbells or "lobes" in opposite directions. Over repeated and rapid rotations, the accumulated effect of displacing these fluid pockets is sufficient to induce a net flow. This motion is illustrated in Fig. 1, where clockwise rotation of the top lobe combined with counterclockwise rotation of the bottom lobe induces flow from left to right. In these experiments, each of the lobes consisted of two independent 3-μm silica spheres (Bangs Laboratories, Fishers, IN). To create these structures, we first maneuvered the colloids with the optical trap to a 3-μm-deep section of channel designed with a region of wider gap to accommodate lobe rotation. Once the particles were properly positioned, the laser was scanned in a manner such that a time-averaged pattern of four independent optical traps was created, one for each microsphere composing the two-lobe pump. By rotating the two traps in the upper part of the channel and the two traps in the lower part of the channel in opposite directions and offset by 90°, the overall pump and the corresponding fluid movement were achieved. Flow direction was easily and quickly reversed by changing the rotation direction of both top and bottom lobes.

To aid visualization of flow and provide a means of estimating flow rate, we added tracer

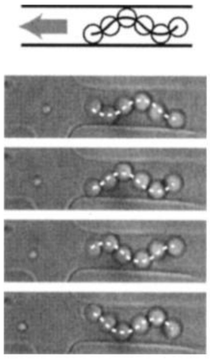

Fig. 3. Three-micrometer colloidal silica used as a peristaltic pump, operating at 2 Hz, to induce flow from right to left within a 6-μm channel. Frames are separated by four cycles to show movement of the 1.5-μm tracer particle.

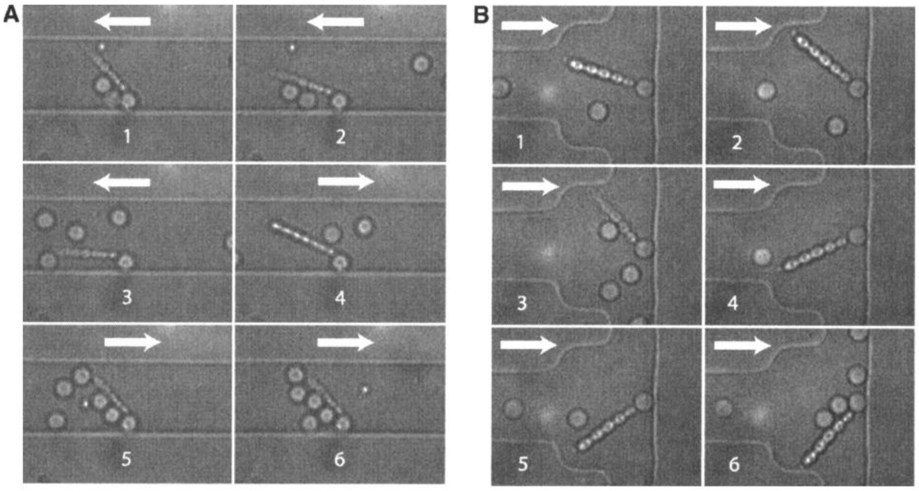

Fig. 4. (A) A passive colloidal valve, where arrows indicate the direction of fluid flow. In images 1 to 3, a flow of ~2 nl/hour pushes the valve arm against the channel wall, allowing particulates in the flow to pass. In images 4 to 6, the flow is reversed, swinging the valve structure across the channel, restricting the flow of the 3-μm colloids but not the smaller 1.5-μm tracer particles. The aqueous solution used to photopolymerize the valve structure consisted of an aqueous monomer, 1.99 M acrylamide (Sigma-Aldrich) and cross-linker solution, 0.048 M bis-acrylamide (Sigma-Aldrich), containing both a photoinitiator, 0.0006 M triethanolamine (J. T. Baker, Phillipsburg, NJ), and a coinitiator, 0.0002 M riboflavin 5′ phosphate sodium salt (Sigma-Aldrich). This solution was pumped into the microfluidic channel network through a syringe pump. Initially fabricated in a deeper region of the network, the linear structures were optically maneuvered into an 11-μm-wide and 3.2-μm-deep straight section of the PDMS microfluidic channel. (B) An actuated, three-way colloidal valve. Images 1 to 3 show the valve structure in a position to direct 3-μm spheres to the lower channel with flow rates of ~2 nl/hour. In images 4 to 6, the valve is moved downward to direct particulates to the upper channel.

particles consisting of 1.5-μm silica spheres to the aqueous solution (Movie S1). The measured tracer particle velocities were determined as a function of the gear rotation rate both in the forward and reverse directions and indicate a maximum flow rate of 1 nl/hour. The dependence appears to be linear and independent of direction, as expected from the laminar nature of the flow (Fig. 2). From the measured tracer particle velocities, we estimate that pressure drops of ~30 μm H_2O are achievable at our fastest rotation rates.

The gear pump design illustrates the success of positive-displacement pumping through the use of colloidal microspheres; however, its design may prove particularly harsh to certain solutions. Although we have been able to pump individual cells using the gear pump (Movie S2), concentrated cellular suspensions may be damaged by the aggressive motion of the meshing "gears" of the pump. We have therefore investigated a second approach that incorporates a peristaltic design also based on the concept of positive fluid displacement, effectively a pseudo two-dimensional analog of a three-dimensional, macroscopic screw pump. If instead of rotating the particles as in the gear pump, they are translated back and forth across the channel in a cooperative manner, fluid propagation can be achieved.

The colloidal movement required to direct flow with this approach is illustrated in Fig. 3. The optical trap moves the colloids in a propagating sine wave within which a plug of fluid is encased. Direction of the flow can be reversed by changing the direction of colloidal wave movement. Again, these experiments were performed with independent, 3-μm silica spheres; however, a larger number of particles was used in the experiments shown in Fig. 3 to represent a complete wavelength. Fabrication of these pumps required first maneuvering the colloids into the channel section. Once in place, the optical trap was scanned such that multiple independent traps were created, one for each colloid composing the peristaltic pump. Tracer particles were also used in these experiments and indicate that comparable flow rates could be achieved with this approach. The "snake-like" motion of this pump is best viewed as movie clips (Movies S3 and S4).

The physical, colloid-based, in situ positive-displacement pumping scheme of these two pumps has a number of advantages in addition to its diminutive size. Because colloidal particles are used, and depending on the design, the actuation scheme could be electrophoretic, magnetophoretic, or optical based. This range of actuation schemes will allow pumping of complex suspensions and nonpolar organic solvents, two fluid classes in which electrophoretic pumping techniques falter or fail.

To restrict and direct the flow of cells or colloids within microfluidic networks, we created two types of valve (Fig. 4) by using laser-initiated photopolymerization to first lock colloids into specific geometries. Once polymerized, these structures are positioned and, in some cases, actuated by the same laser used for their construction. Each valve consists of a 3-μm silica sphere photopolymerized to several 0.64-μm silica spheres that form a linear structure. For passive applications, the device was maneuvered into a straight channel and the 3-μm sphere was held next to the wall, allowing the arm to rotate freely in the microchannel. As the flow direction was changed (Fig. 4A), the valve selectively restricted the flow of large particles in one direction while allowing passage of all particles in the other. To actively direct particulates to one of two exit channels, the passive valve was maneuvered into a confining "T" geometry. As the valve structure was rotated about its swivel point by using the optical trap, the top or bottom channel was sealed, directing flow of particulates toward the open channel (Fig. 4B) (Movies S5 and S6).

We have shown here that colloidal particles can be used to fabricate true micrometer-scale microfluidic pumps and valves that are much smaller than those constructed with current approaches (*16*, *27*, *28*). Although the use of an optical trap provides a number of advantages, including the elimination of physical connection to macroscopic hardware and the ability to instantly alter device design or location in situ, actuation of these devices via other applied fields is certainly feasible. As discussed previously, appropriately selected colloids will also translate in applied electric and magnetic fields. Because of its versatility, a colloid-based approach to microfluidic flow generation and control may indeed prove a powerful technique for the creation of complex, highly integrated, microscale total analysis systems.

References and Notes

1. C. S. Effenhauser, A. Manz, H. M. Widmer, *Anal. Chem.* **65**, 2637 (1993).
2. P. Wilding, M. A. Shoffner, L. J. Kricka, *Clin. Chem.* **40**, 1815 (1994).
3. G. M. Whitesides, A. D. Stroock, *Phys. Today* **54**, 42 (June 2001).
4. A. E. Kamholz, B. H. Weigl, B. A. Finlayson, P. Yager, *Anal. Chem.* **71**, 5340 (1999).
5. P. J. A. Kenis, R. F. Ismagilov, G. M. Whitesides, *Science* **285**, 83 (1999).
6. R. P. Hertzberg, A. J. Pope, *Curr. Opin. Chem. Biol.* **4**, 445 (2000).
7. R. F. Service, *Science* **282**, 400 (1998).
8. A. van den Berg, W. Olthuis, P. Bergveld, *Micro Total*

Analysis Systems 2000 (Kluwer Academic, Dordrecht, Netherlands, 2000).
9. S. Shoji, M. Esashi, *J. Micromech. Microeng.* **4**, 157 (1994).
10. S. F. Bart, L. S. Tarrow, M. Mehregany, J. H. Lang, *Sensors Actuators A* **21–23**, 193 (1990).
11. A. Manz *et al.*, *J. Micromech. Microeng.* **4**, 257 (1994).
12. D. E. Kataoka, S. M. Troian, *Nature* **402**, 794 (1999).
13. B. Zhao, J. S. Moore, D. J. Beebe, *Science* **291**, 1023 (2001).
14. E. W. H. Jager, O. Inganas, I. Lundstrom, *Science* **288**, 2335 (2000).
15. A. Hatch, A. E. Kamholz, G. Holman, P. Yager, K. F. Boehringer, *J. Microelectromech. Syst.* **10**, 215 (2001).
16. M. A. Unger, H.-P. Chou, T. Thorsen, A. Scherer, S. R. Quake, *Science* **288**, 113 (2000).
17. R. C. Gauthier, R. N. Tait, H. Mende, C. Pawlowicz, *Appl. Opt.* **40**, 930 (2001).
18. S. Maruo, K. Ikuta, K. Hayato, in *Proceedings of the 14th Annual IEEE International Conference on MEMS* (IEEE, Piscataway, NJ, 2001), pp. 594–597.
19. S. M. Kuebler *et al.*, in *Micro- and Nano-Photonic Materials and Devices*, J. W. Perry, A. Scherer, Eds. (International Society for Optical Engineering, Bellingham, WA, 2000), pp. 97–105.
20. P. Galajda, P. Ormos, *Appl. Phys. Lett.* **78**, 249 (2001).
21. S. Kawata, H.-B. Sun, T. Tanaka, K. Takada, *Nature* **412**, 697 (2001).
22. C. Mio, T. Gong, A. Terray, D. W. M. Marr, *Rev. Sci. Instrum.* **71**, 2196 (2000).
23. C. Mio, D. W. M. Marr, *Adv. Mater.* **12**, 917 (2000).
24. D. C. Duffy, O. J. A. Schueller, S. T. Brittain, G. M. Whitesides, *J. Micromech. Microeng.* **9**, 211 (1999).
25. J. C. McDonald *et al.*, *Electrophoresis* **21**, 27 (2000).
26. D. C. Duffy, J. C. McDonald, O. J. A. Schueller, G. M. Whitesides, *Anal. Chem.* **70**, 4974 (1998).
27. D. J. Beebe *et al.*, *Nature* **404**, 588 (2000).
28. Q. Yu, J. M. Bauer, J. S. Moore, D. J. Beebe, *Appl. Phys. Lett.* **78**, 2589 (2001).
29. Supported by the NSF (grants CTS-9734136 and CTS-0097841) and the Office of Life and Microgravity Sciences and Applications, NASA (grant NAG9-1364). We thank T. Vestad and N. Flannery for their assistance with device fabrication and Y. Munakata for useful discussions.

Supporting Online Material
www.sciencemag.org/cgi/content/full/296/5574/1841/DC1
Movies S1 to S6

22 March 2002; accepted 30 April 2002

The Origin of Cu/Au Ratios in Porphyry-Type Ore Deposits

Werner E. Halter,* Thomas Pettke, Christoph A. Heinrich

Microanalysis of major and trace elements in sulfide and silicate melt inclusions by laser-ablation inductively coupled plasma mass spectrometry indicates a direct link between a magmatic sulfide liquid and the composition of porphyry-type ore deposits. Copper (Cu), gold (Au), and iron (Fe) are first concentrated in a sulfide melt during magmatic evolution and then released to an ore-forming hydrothermal fluid exsolved late in the history of a magma chamber. The composition of sulfide liquids depends on the initial composition and source of the magma, but it also changes during the evolution of the magma in the crust. Magmatic sulfide melts may exert the dominant direct control on the economic metal ratios of porphyry-type ore deposits.

Magmatic-hydrothermal ore deposits in porphyry stocks are the world's most important source of Cu and Mo and a significant source of Au, and their profitable exploitation often depends on a combined recovery of several metals. Porphyry deposits form through pervasive veining and alteration of intermediate to acid (that is, silica-rich) intrusions by magmatic-hydrothermal aqueous fluids, exsolved from a subjacent magma reservoir (*1*). This fluid mobilizes metals from several cubic kilometers of magma and transports them to the depositional site within a short period of time. Ore minerals precipitate from the fluid upon cooling and interaction with solidified rock. The relative proportions of ore metals (Cu, Au, and Mo) in porphyry-type deposits are variable, and systematic criteria to explain this variation are difficult to isolate (*2*). Crustal magmatic processes may have an important influence on metal ratios, whereas hydrothermal precipitation within the porphyry vein network appears not to strongly fractionate chemically similar metals such as Cu and Au (*3*, *4*). Therefore, the key to the genesis and composition of economic porphyry-type ore deposits lies in the processes controlling the composition of the magmatic volatile phase.

To understand the exsolution of the mineralizing fluid and the transfer of ore metals from the magma to the volatile phase, we are investigating the igneous history of ore-forming calcalkaline systems. Primary melt inclusions (MIs) in phenocrysts preserve the magmatic record despite pervasive hydrothermal alteration of the rock matrix. MIs are small droplets (5 to 50 µm in diameter) of magmatic liquids trapped during the growth of minerals. Silicate liquid is commonly recorded in MIs, but sulfide liquids were also discovered in certain rocks (Fig. 1). After extensive petrographic study, we used laser-ablation inductively coupled plasma mass spectrometry (LA-ICPMS) to analyze the major and trace element content of entire unexposed MIs (*5*). Integrated analysis of inclusions by laser sampling is essential in the case of sulfide melts, which never quench to a homogeneous glass. Our study focused on the Farallón Negro Volcanic Complex in northwestern Argentina, hosting the large Bajo de la Alumbrera porphyry Cu-Au deposit (*4*, *6*–*9*).

Most major and trace elements in silicate MIs follow the differentiation trend defined by bulk rock compositions, except for Cu, which varies at all stages of magmatic evolution (Fig. 2). Cu concentrations in silicate MIs in phenocrysts from volcanic rocks are one to two orders of magnitude higher [$\sim$100 to 3000 parts per million by weight (ppm)] than in the bulk rocks ($\sim$10 to 50 ppm). This shows that the evolving melt composition was more Cu-rich than common calcalkaline rocks [10 to 150 ppm (*10*)] before the transfer of Cu to the magmatic volatile phase and its dispersion during volcanic eruption (*11*). In the subvolcanic intrusions, MIs with $<$65 weight % (wt %) SiO_2 are depleted in Cu ($\sim$2 to 3 ppm and often below the limit of detection). These silicate MIs are hosted by amphibole and coexist with small (1 to 10 µm in diameter) and irregularly shaped primary sulfide MIs (Fig. 1), documenting the fact that basic to intermediate melts forming the mafic phenocrysts of intrusive rocks had exsolved a sulfide liquid. No sulfide inclusions occur in phenocrysts of the extrusive rocks nor in plagioclase phenocrysts containing silica-rich MIs in the intrusive rocks (Fig. 2).

Sulfide MIs were analyzed by LA-ICPMS for their Fe, Cu, and Au contents. Analyses and signal quantification were conducted according

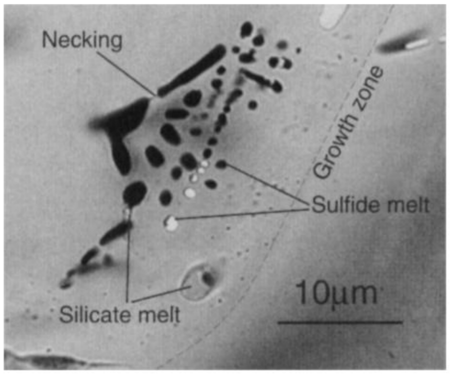

Fig. 1. Microphotograph of MIs, trapped in magmatic amphibole from intrusive rocks. The globular shape and necking of the sulfides are evidence for trapping at a molten stage, in equilibrium with a coexisting silicate melt. The image was taken in transmitted and reflected light, the latter rendering sulfide MIs bright white when exposed to the sample surface. Only entire subsurface inclusions (appearing black) were studied by quantitative LA-ICPMS microanalysis.

Isotope Geochemistry and Mineral Resources, Department of Earth Sciences, Swiss Federal Institute of Technology (ETH), ETH Zentrum NO, 8092 Zürich, Switzerland.

*To whom correspondence should be addressed. E-mail: halter@erdw.ethz.ch